Received 25 July 2022; revised 17 August 2022; accepted 19 August 2022. Date of publication 31 August 2022; date of current version 16 September 2022.

Digital Object Identifier 10.1109/OJAP.2022.3203250

Bandwidth Enhancement of Millimeter-Wave Large-Scale Antenna Arrays Using X-Type Full-Corporate Waveguide Feed Networks

FANQI SUN [1] (Student Member, IEEE), YUJIAN LI [1] (Member, IEEE), JUNHONG WANG [1] (Senior Member, IEEE), LEI GE [2] (Senior Member, IEEE), JIANXIN CHEN [3] (Senior Member, IEEE), AND WEI QIN [3] (Member, IEEE)

[1]Key Laboratory of All Optical Network and Advanced Telecommunication Network, Ministry of Education, Beijing Jiaotong University, Beijing 100044, China

[2]College of Electronic Science and Technology, Shenzhen University, Shenzhen 518060, China

[3]School of Electronics and Information, Nantong University, Nantong 226019, China

CORRESPONDING AUTHOR: Y. LI (e-mail: liyujian@bjtu.edu.cn)

This work was supported in part by the National Key Research and Development Program of China under Grant 2021YFA0717500; in part by the National Natural Science Foundation of China under Grant 62271038 and Grant 62031004; and in part by the Dongguan University of Technology under Grant KCYKYQD2017007.

ABSTRACT A one-time-reflection equivalent model of the full-corporate waveguide feed networks is investigated to propose a novel approach to bandwidth enhancement of millimeter-wave large-scale antenna arrays. Theoretical analysis reveals that the in-phase superposition phenomenon of multiple small reflections at specific frequencies caused by the topology of the feed network is also a significant factor to affect the achievable bandwidth of the large-scale arrays, apart from the bandwidth performance of the individual power dividers and radiators composing the array. In order to weaken the undesirable effects on bandwidths caused by the small reflections, a full-corporate waveguide feed network with an X-type topology is then presented. Air-filled waveguide X-junctions and waveguide-fed horn sub-arrays are designed to fulfill new three-dimensional (3D) printed V-band antenna arrays. Excellent performance, including an improved bandwidth of about 40%, a gain of up to 27.8 dBi, and stable unidirectional radiation patterns with cross polarization of less than -32 dB, are confirmed experimentally by an 8×8 prototype. The theoretical model and the bandwidth enhancement scheme in this paper are valuable to realize the high-gain wideband antenna arrays for emerging millimeter-wave applications.

INDEX TERMS Millimeter-wave, 3D-printed, antenna array, full-corporate feed network, wideband, high gain.

I. INTRODUCTION

MILLIMETER-WAVE communications are of great importance to various emerging applications with the need of ultra-high data transmission rate, including virtual reality (VR), virtual assistants, augmented reality (AR), advanced mobile devices and so on [1], [2], [3], [4]. In order to guarantee the wireless link budget and to effectively use the plentiful spectrum, a great deal of attention has been dedicated to enhancing both the gain and bandwidth of millimeter-wave antenna arrays [5].

A high radiation efficiency is required for increasing the gain of arrays. Several methods, including the air substrate [6], the bandgap structures [7], and the backed cavities [8], have been introduced to the antenna elements to suppress the undesirable surface waves travelling along radiating apertures that affected the array efficiency. Meanwhile, it has been verified that for an array with a large scale, the loss of the feed network was the main reason for restricting the achievable gain of the array [9]. Therefore, in comparison with the feed networks consisting of substrate integrated

transmission lines [10], [11], [12], [13], [14], the air-filled waveguide feed networks without the dielectric losses were a better choice for the array design with a gain of above 30 dBi [15], [16], [17], [18], [19], [20].

In respect of the array bandwidth enhancement, wideband antenna elements and feed networks were two approaches that have been persistently investigated in the literature. Since the millimeter-wave slot [21], cavity [22] and microstrip patch [6] antennas in an early stage usually suffered from narrow bandwidths, more efforts were focused on widening the bandwidth of radiating elements [23], [24], [25]. With the assistant of different types of millimeter-wave antennas with broadened bandwidths of more than 20% that were fed by traditional full-corporate feed networks, the array bandwidths with relatively stable radiation characteristics were increased from about or even less than 10% to around 20% [26], [27], [28], [29], [30].

In order to improve the array bandwidth in a further step, feed networks with wider bandwidths were necessary as well, and thus have also been studied. For the widely used full- corporate feed networks with an H-type topology [10], [15], T-junctions operating as cascaded power dividers played a crucial role in the bandwidth improvement. Additional metallic pins [31], [32] and irises [20], [33], [34] were employed in the design of H-plane substrate-integrated and air-filled waveguide T-junctions to extend their operating bandwidths. Meanwhile, stepped or tapered waveguide structures are another kind of scheme to improve the impedance matching of both E-plane [16], [35] and H-plane [36] waveguide T-junctions. Benefiting from those wideband waveguide T-junctions, bandwidths of more than 30% have been achieved by several millimeter-wave arrays with promising radiation performance [16], [31], [32], [33], [35], [36], [37]. Unfortunately, a bandwidth of 40% that is desirable for the fifth generation (5G) millimeter-wave multi-band applications was still a challenge in the reported high-gain arrays with large scales. Recently, a Ka-band parallel-feed continuous transverse stub array was designed in [38], which realized a bandwidth of 40% and a gain close to 30 dBi. However, the relatively complex geometry was not flexible for the array design with a larger scale. On the other hand, the bandwidth of a parallel feed network consisting of microstrip lines was enhanced to more than 40% by considering the whole network as a continuous impedance transition device [39]. Moreover, a 4×4 microstrip line fed magneto-electric (ME) dipole array on LTCC with a bandwidth of 45% was reported in [40]. Nevertheless, as aforementioned, those feed networks based on the TEM-mode substrate-integrated transmission lines were not promising for the high-gain requirements. The continuous impedance transformation in the entire air-filled waveguide feed network was not easy to realize as well.

For the purpose of further enhancing the bandwidth of the millimeter-wave antenna arrays with air-filled feed networks, a study based on the one-time-reflection circuit model [41] is implemented to analyze the impedance matching features of the full-corporate feed network in this paper. It reveals that apart from the reflections of the separated power dividers and the radiators, the in-phase superposition of the small reflections in the full-corporate feed network is another factor restricting the array bandwidth, especially for the large-scale arrays. To overcome the issue, a revised full-corporate feed network topology constructed by air-filled X-junctions rather than T-junctions is then presented, investigated, and used for designing a 60-GHz high-gain wideband horn array that is fabricated by employing the metallic three-dimensional (3D) printing technology [42], [43], [44]. The results and the proposed array in this work are valuable to the bandwidth enhancement of millimeter-wave large-scale antenna arrays.

The paper is organized as follows. Section II depicts the theoretical analysis on the full-corporate feed networks. Section III designs the wideband horn antenna array in the V-band. Measured results and discussions are given in Section IV. Eventually, a brief conclusion is presented in Section V.

II. THEORETICAL ANALYSIS ON BANDWIDTH ENHANCEMENT

Millimeter-wave antenna arrays with full-corporate waveguide feed networks are usually composed of radiating elements, feeding cavities acting as sub-array feed networks, and the major full-corporate feed networks, which are located in the upper, middle and lower layers of the designs respectively [9], [15], [17]. In this section, a simplified one-time-reflection circuit model of the full-corporate feed network is developed based on the theory of small reflections [41], which provides an effective means to analyze the reflection characteristics of the full-corporate feed networks with arbitrary sizes. With the help of the model, a method of enhancing the bandwidth of large-scale waveguide feed networks is then discussed.

A. ONE-TIME-REFLECTION MODEL OF THE FULL-CORPORATE FEED NETWORK

The topology of the conventional H-type full-corporate feed network consisting of a series of T-junctions is shown in Fig. 1 (a). The output ports of the feed network are connected with 2×2 sub-arrays that are considered as the loads of the feed network in this model. As the transmitting paths from the input port to all output ports are parallel to each other, the feed network can be equivalent to a cascade network as depicted in Fig. 1 (b), where the load Z_L represents the sub-array. Clearly, a feed network with a size of $2^N \times 2^N$ is used for exciting an array with a size of $2^{N+1} \times 2^{N+1}$, while the number of T-junctions constructing the cascade network is $2N$. Meanwhile, the path length l_i between two neighboring T-junctions can be expressed as

$$l_i = \begin{cases} d \cdot 2^{N-\frac{i+1}{2}}, & \text{if } i \text{ is odd} \\ d \cdot 2^{N-\frac{i}{2}}, & \text{if } i \text{ is even} \end{cases} \quad (1 \le i \le 2N, i \in Z) \quad (1)$$

where d is the element spacing of the antenna array.

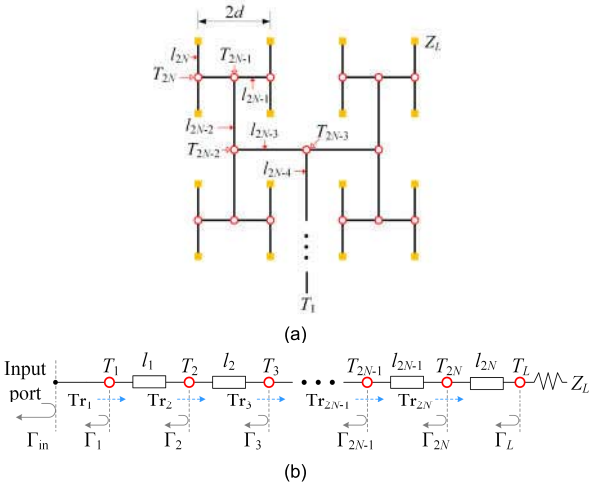

FIGURE 1. H-type full-corporate feed network. (a) Topology of the feed network, (b) simplified one-time-reflection model of the feed network.

As illustrated in Fig. 1 (b), due to the discontinuities caused by the T-junctions, small reflections would exist in the feed network. In this study, only the one-time-reflections from the T-junctions are considered and the loss of the feed network is omitted. The promising accuracy of the simplified model will be confirmed later. Therefore, the total reflection coefficient at the input port of the feed network Γ_{in} can be calculated as

$$\Gamma_{\text{in}} = \Gamma_1 + \sum_{i=2}^{2N}\left(\Gamma_i \cdot e^{-2\text{j}\theta_{i-1}} \cdot \prod_{2}^{i} \text{Tr}_{i-1}\right) + \Gamma_L \cdot e^{-2\text{j}\theta_{2N}} \cdot \prod_{1}^{2N} \text{Tr}_i \tag{2}$$

where Γ_i and Tr_i are the reflection and transmission coefficients for the T-junction T_i. Γ_L is the reflection coefficient of the load. For the one-time-reflection model, Tr_i can be calculated as

$$\text{Tr}_i = 1 + \Gamma_i \tag{3}$$

Then,$\theta_i = \beta L_i$ and β is the propagation constant of the feeding waveguide. L_i is the total path length from the input port of the feed network to the T-junction T_{i+1}, which can be expressed as

$$L_i = l_i + L_{i-1} \tag{4}$$

where $L_0 = 0$.

In order to verify the effectiveness of the one-time-reflection model proposed above, two H-type full-corporate feed networks with sizes of 4 × 4 and 8 × 8 are then analyzed. The corresponding element spacing d of the arrays is set to $0.73\lambda_c$, where λ_c is the cutoff wavelength for the TE_{10} mode of the waveguide in the feed networks.

The H-plane air-filled waveguide T-junctions used for the feed networks have the same geometry with Design A in [44]. A full-wave electromagnetic solver Ansys HFSS [45] is employed to determine the simulated reflection and transmission coefficients of the T-junctions, which are then introduced in the model as Γ_i and Tr_i to calculate Γ_{in} of the feed networks. Besides, Γ_L is set to 0 in this section. The simulated Γ_i of the T-junctions and the calculated $|\Gamma_{in}|$ of the feed networks are plotted in Figs. 2 (a) and (b). On the other hand, the overall geometry of the two feed networks is modeled and simulated in the full-wave electromagnetic solver as well, whose simulated $|\Gamma_{in}|$ results are provided in Fig. 2 (b) for comparison. It is noted that only the frequency range supporting the single TE_{10} mode in the rectangular waveguide, namely f/f_c varying from 1 to 2, is considered here. Clearly, a good agreement between the calculated and simulated reflection coefficients of the feed networks can be observed in Fig. 2 (b), which demonstrates the promising accuracy of the presented one-time-reflection model for evaluating the reflection characteristics of the full-corporate feed networks.

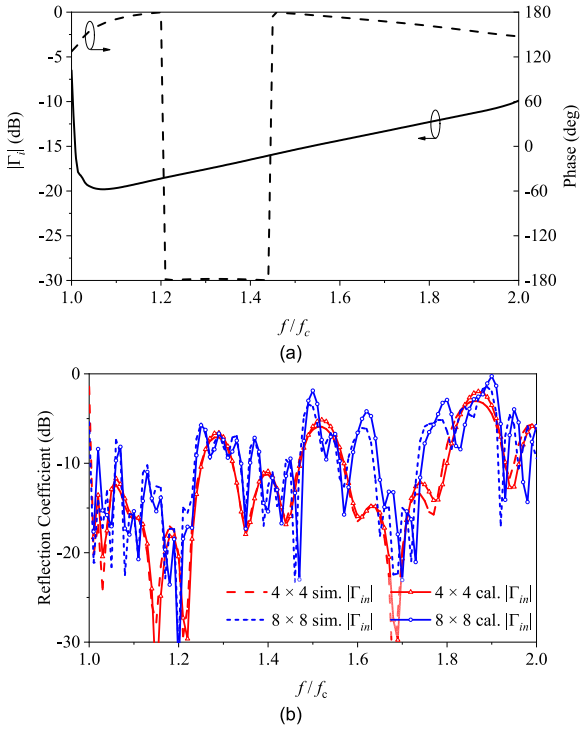

FIGURE 2. Simulated and calculated reflection coefficients of the used T-junctions and the H-type air-filled waveguide feed networks with sizes of 4 × 4 and 8 × 8. (a) T-junctions, (b) feed networks.

B. REFLECTION CHARACTERISTICS OF THE H-TYPE FEED NETWORK

With the use of the one-time-reflection model proposed in the above section, the reflection characteristics of the H-type feed network are investigated in a further step in this section. For better revealing the influence of the feed network topology on the reflection features, the magnitudes and phases of the reflection coefficients of the T-junctions and the loads are set to fixed values −20 dB and 180° over the considered frequency range. In addition, d still equals to $0.73\lambda_c$.

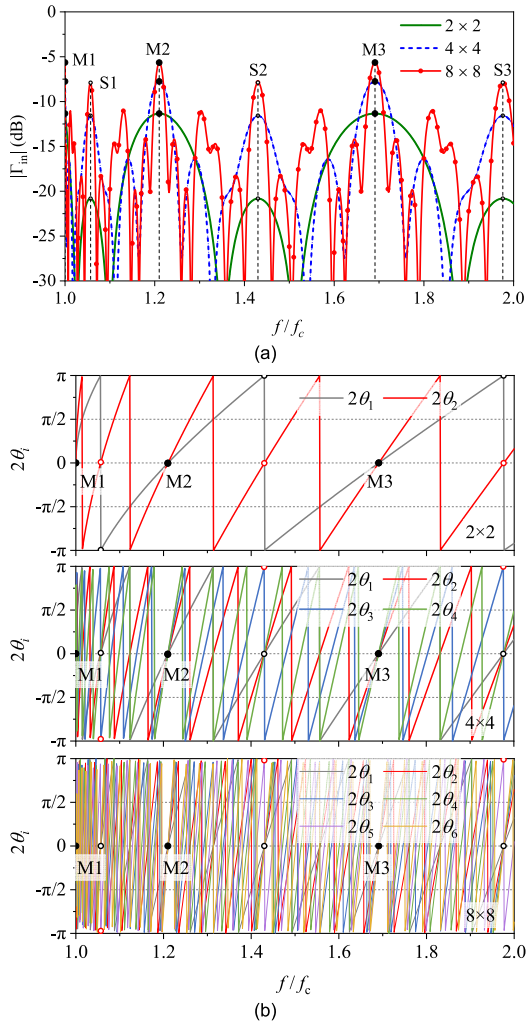

FIGURE 3. Calculated results of the H-type full-corporate feed networks with sizes of 2 × 2, 4 × 4 and 8 × 8 when $|\Gamma_i| = |\Gamma_L| = -20$ dB. (a) $|\Gamma_{in}|$, (b) $2\theta_i$.

Fig. 3 (a) presents the calculated $|\Gamma_{in}|$ of the feed networks with three different sizes. It is seen that although Γ_i and Γ_L are constant, $|\Gamma_{in}|$ varies significantly with the frequency. More null points can be observed on the $|\Gamma_{in}|$ curve for the feed network with a larger size. Meanwhile, the peak values of $|\Gamma_{in}|$ also increase with the size of the feed network, which appear at fixed frequencies. Specifically, the frequencies with the largest values of $|\Gamma_{in}|$ are marked as M1, M2 and M3, while the frequencies with the second largest values of $|\Gamma_{in}|$ are marked as S1, S2 and S3 in Fig. 3 (a). Therefore, it is found that apart from the individual T-junctions, the overall topology of the full-corporate feed networks is another factor affecting their impedance matching. Due to the increased peak values of $|\Gamma_{in}|$ discussed above, the bandwidth enhancement is a tougher task for the feed network with a larger size.

For the purpose of exploring the reason for the increased $|\Gamma_{in}|$ at specific frequencies, the calculated phase delay from the input port of the feed network to each T-junction θ_i is depicted in Fig. 3 (b). At the normalized frequencies of 1, 1.21 and 1.69, corresponding to M1, M2 and M3 shown in Fig. 3 (a), θ_i equals 0 for all the T-junctions. As a result, the small reflections from the T-junctions are in-phase at the input of the feed network, which leads to the maximum reflections. Moreover, the in-phase superposition of the small reflections can be achieved at the normalized frequencies of 1.06, 1.43 and 1.98, namely S1, S2 and S3 in Fig. 3 (a), for all the T-junctions save for one with the out-of-phase reflection, which results in the second largest values of $|\Gamma_{in}|$ over the frequency range of interest. According to (1) and (2), for the H-type feed networks, the frequencies satisfying the in-phase superposition condition of the small reflections are determined by the element spacing d and the propagation constant of the waveguide β. However, it is found in the study that with the existence of the practical waveguide T-junctions, the equivalent transmitting path length for each T-junction is slightly shorter than the physical length calculated by using (1) and (4), which has been considered in the calculation in Fig. 2 to get a better accuracy, but is ignored in the analysis in Fig. 3 for simplification. Therefore, the frequencies with the peak values of $|\Gamma_{in}|$ for the feed networks discussed in this and last sections having the same d and β are slightly different with each other. The detailed frequency values are listed in Table 1 for comparison.

TABLE 1. Comparison of the detailed frequency values for the theoretical and practical H-type full-corporate feed network models.

	M1	S1	M2	S2	M3	S3
Theoretical	1	1.06	1.21	1.43	1.69	1.98
4 × 4	1	1.07	1.28	1.52	1.87	
8 × 8	1	1.07	1.3	1.55	1.9	

Based on the aforementioned analysis, it is confirmed that apart from designing wideband T-junctions that has been widely addressed in the literature, the influence of the topology of the full-corporate feed networks is also worth considering for enhancing the bandwidth of arrays. Actually, it may be of more importance for widening the bandwidth of large-scale arrays, considering the achievable impedance matching features of the individual T-junctions.

C. BANDWIDTH ENHANCEMENT METHOD

By employing the idea revealed in the last section for the bandwidth enhancement of the arrays, two full-corporate feed networks with the revised topology are investigated in this section, which are illustrated in Figs. 4 (a) and (b), separately. Both d and β of them are kept the same with those in the last section.

Different from the conventional H-type feed network, a half of the T-junctions indicated in Fig. 1 (a) is replaced with the 1-to-4 power dividers shown in Fig. 4 (a). Another half of the T-junctions are separated into two right angle transmission lines. The X-shaped junctions are then introduced in the feed network depicted in Fig. 4 (b). By the means, half of the T-junctions in the H-type feed network can be saved, and thus the number of nodes with small

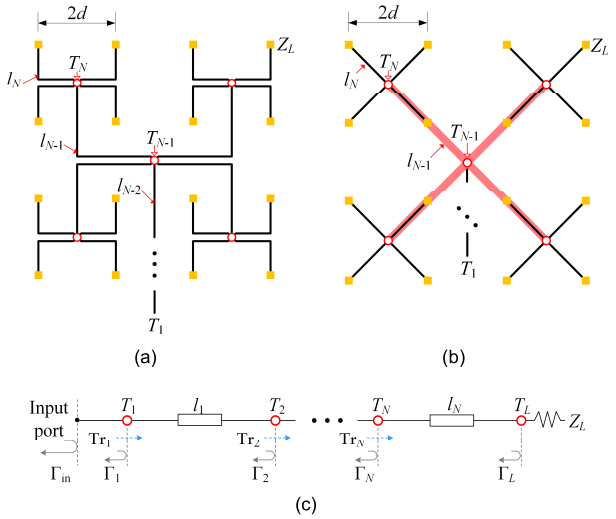

FIGURE 4. Full-corporate feed networks with the modified topologies. (a) H-type feed network composed of 1-to-4 power dividers, (b) X-type feed network, (c) one-time-reflection model of the feed network with the modified topologies.

reflections in the one-time-reflection model of the modified feed network with a size of $2^N \times 2^N$ is N as shown in Fig. 4 (c). Consequently, the total reflection coefficient at the input port of the revised feed networks Γ_{in} is calculated as

$$\Gamma_{\text{in}} = \Gamma_1 + \sum_{i=2}^{N}\left(\Gamma_i \cdot e^{-2\text{j}\theta_{i-1}} \cdot \prod_{2}^{i} \text{Tr}_{i-1}\right) + \Gamma_L \cdot e^{-2\text{j}\theta_N} \cdot \prod_{1}^{N} \text{Tr}_i \tag{5}$$

Meanwhile, the path length l_i between the neighboring two T-junctions is extended and can be expressed as

$$l_i = d \cdot 2^{N-i+1} (1 \le i \le N, i \in Z) \tag{6}$$

for the feed network in Fig. 4 (a) and

$$l_i = d \cdot 2^{N-i+\frac{1}{2}} (1 \le i \le N, i \in Z) \tag{7}$$

for the feed network in Fig. 4 (b).

Three different kinds of full-corporate feed networks with the same size of 4 × 4, including the conventional H-type, the H-type composed of 1-to-4 power dividers, and the X-type, are analyzed, whose calculated $|\Gamma_{in}|$ results based on the one-time-reflection models are compared in Fig. 5 (a). First, in comparison with the results of the traditional H-type design, the H-type feed network consisting of the 1-to-4 power dividers has a lower maximum value of $|\Gamma_{in}|$, because the reduced number of the junctions weakens the in-phase superposition of the small reflections for the feed network with a fixed size. However, due to the same transmission paths for the small-reflections, the frequencies with the peak values of $|\Gamma_{in}|$ are not changed for the two H-type feed networks. Second, by replacing the 1-to-4 power dividers constructing the H-type feed network

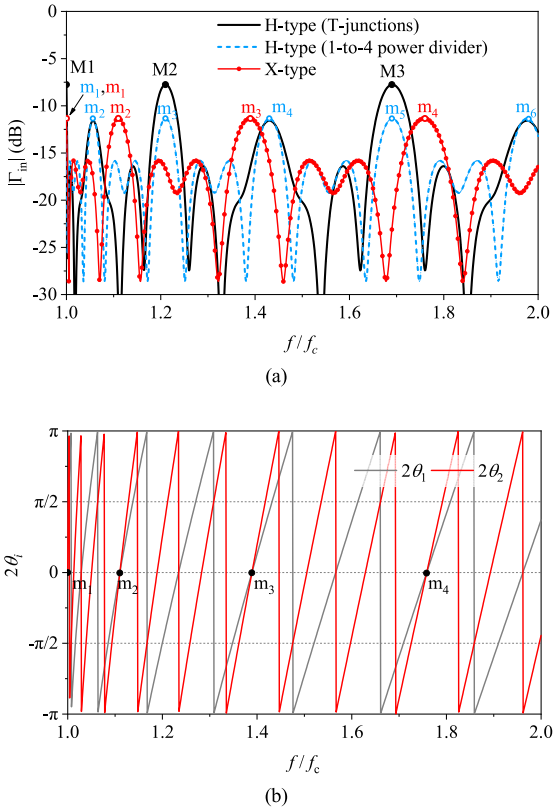

FIGURE 5. Calculated results of the three types of full-corporate feed networks with a size of 4 × 4 when $|\Gamma_i| = |\Gamma_L| = -20$ dB. (a) $|\Gamma_{in}|$ and (b) $2\theta_i$ for the proposed X-type feed network.

with the X-junctions, the path lengths between junctions are shortened, which makes the peak values of $|\Gamma_{in}|$ move to higher frequencies as exhibited in Fig. 5 (a). The calculated θ_i results for the X-type feed network are given in Fig. 5 (b), which confirms that the in-phase superposition occurs at the normalized frequencies 1, 1.11, 1.39, 1.76, respectively. Therefore, it is seen that the reduction in the path lengths of the small-reflections is helpful to decrease the number of points with the peak values of $|\Gamma_{in}|$ within a fixed frequency range.

The effect of the reflection coefficients Γ_i and Γ_L on the impedance matching of the X-type full-corporate feed network are then considered in Fig. 6. It is noted that when Γ_i or Γ_L varies, the other one is fixed to −20 dB. As shown in Fig. 6, although different of Γ_i or Γ_L does not vary the frequencies with the peak values of $|\Gamma_{in}|$ for the feed network, but $|\Gamma_{in}|$ around those frequencies varies significantly with Γ_i and Γ_L. Clearly, Γ_i and Γ_L, which are determined by the specific designs of power dividers and sub-arrays in practice, are not constant within the frequency range of interest. Therefore, smaller Γ_i and Γ_L around the frequencies with the in-phase superposition of small reflections are desirable for guaranteeing an acceptable $|\Gamma_{in}|$ throughout a wide band. Otherwise, the bandwidth of the feed network is difficult to enhance due to the existence of the strong reflection points.

Fig. 7 provides the relation between $|\Gamma_i|$ and $|\Gamma_L|$ under the condition of $|\Gamma_{in}| \le -10$ dB for the H-type and X-type feed

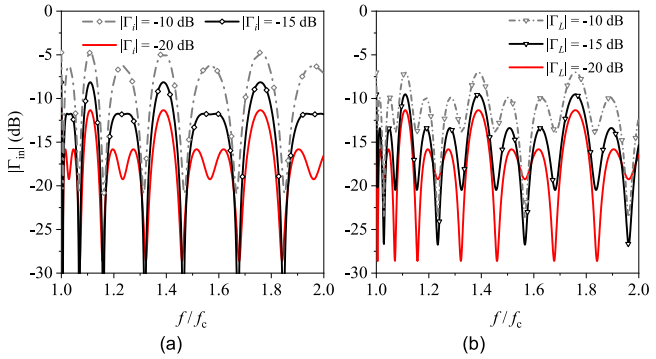

FIGURE 6. Simulated $|\Gamma_{in}|$ of the 4 × 4 X-type feed network for different (a) Γ_i and (b) Γ_L.

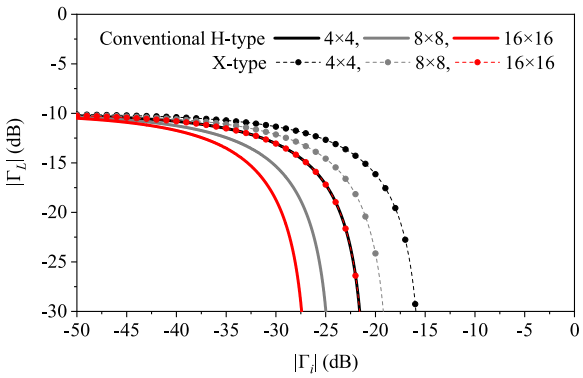

FIGURE 7. The relation between $|\Gamma_i|$ and $|\Gamma_L|$ under the condition of $|\Gamma_{in}| \leq -10$ dB for the H-type and X-type feed networks with different sizes.

networks with different sizes over the entire frequency range supporting the single transmission mode. Due to smaller reflection nodes existing in the feed networks with a larger size, lower $|\Gamma_i|$ and $|\Gamma_L|$ are required for realizing $|\Gamma_{in}| \leq -10$ dB. More importantly, taking advantage of decreasing the maximum values of $|\Gamma_{in}|$ discussed in the last section, the required $|\Gamma_i|$ and $|\Gamma_L|$ for getting $|\Gamma_{in}| \leq -10$ dB is easier to fulfill for the X-type feed network compared with that for the H-type one as shown in Fig. 7. According to the aforementioned discussions, it can be summarized that the X-type full-corporate feed network topology that weakens the in-phase superposition effect in the feed network due to small reflections provides a new means to realize the millimeter-wave wideband arrays with large sizes.

III. WIDEBAND LARGE-SCALE ARRAY DESIGN

Based on the bandwidth enhancement scheme investigated in Section II, a novel V-band wideband horn array fed by a multi-layered full-corporate feed network consisting of air-filled waveguide X-junctions is implemented in this section.

A. ARRAY GEOMETRY

An overall hollow configuration of the proposed antenna array is depicted in Fig. 8, which is composed of horn elements, feed cavities and a multi-layered feed

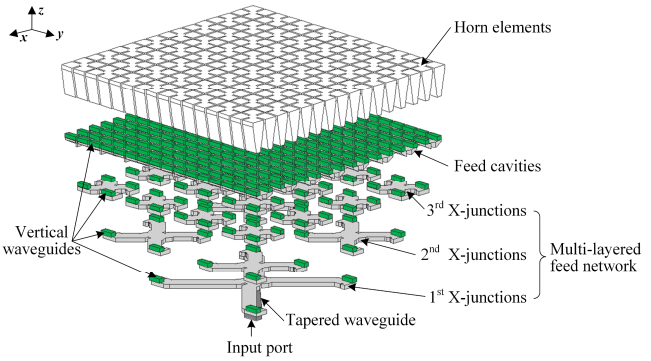

FIGURE 8. Geometry of the proposed 16 × 16 horn antenna array.

network. Four horn elements are combined with a feed cavity to realize a 2 × 2 sub-array, which is seen as the load in the bandwidth enhancement scheme. Moreover, a set of air-filled rectangular waveguide X-junctions with varied sizes are assigned in different layers to prevent the geometric overlap in the X-type full-corporate feed network. By using a series of vertical waveguides with a short length to connect the X-junctions and sub-arrays located in adjacent layers, the input power from a standard WR-15 waveguide port can be transmitted into all radiators successfully with equal-amplitude in-phase excitations. It is noted that the overall thickness of the design increases with the array scale due to the use of the multi-layered X-type feed network. In addition, the minimum printable dimension of about 0.5 mm for the used commercial 3D-printed facility is considered in the design process.

In order to achieve a wide operating band accompanied with promising radiation features, three considerations are addressed in the array design. First, the spacing between neighboring radiation elements is set to 4 mm, corresponding to a wavelength in free space at 75 GHz. Therefore, stable radiation patterns can be maintained by the array within the V-band. Second, the broad wall sizes of the waveguides in the feed network are set to around 3.4 mm, which leads to a single-mode frequency range between 44.1 and 88.2 GHz for the TE_{10} mode. Third, based on the selected element spacing and broad wall sizes, the reflection characteristics of the whole X-type feed network can be assessed by using the model discussed in Section II. It is found in the study that the additional influence of the vertical waveguides on the total transmission path in the feed network should be considered for a promising accuracy. The calculated in-phase superposition of the reflections appears at about 51 and 65.5 GHz for the feed network operating in the V-band. Consequently, the sub-arrays and the X-junctions with small reflection coefficients in the vicinities of the two frequencies would be helpful to realize the wideband antenna array.

B. 2 × 2 SUB-ARRAY

The detailed geometry of the 2 × 2 sub-array is shown in Fig. 9. The four E-plane horn elements have a radiation

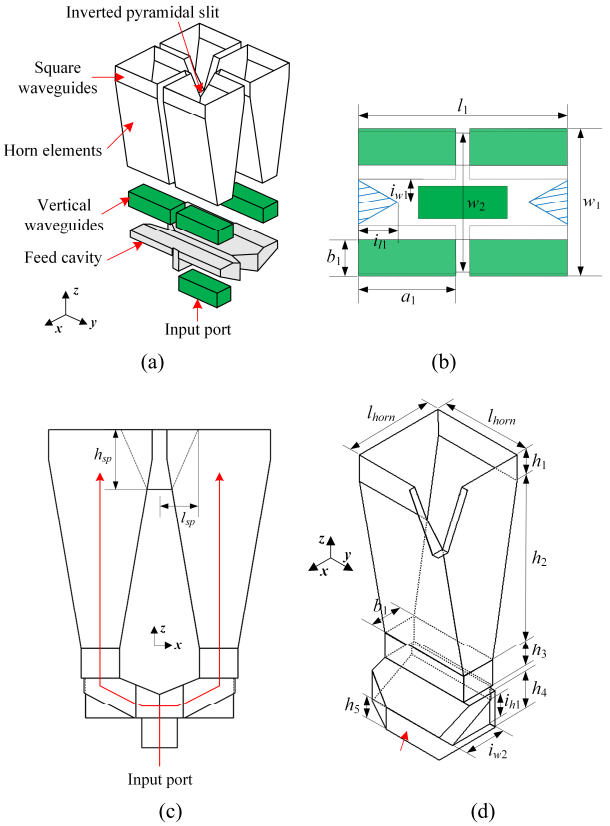

FIGURE 9. Geometry of the 2 × 2 sub-array. (a) Perspective view, (b) top view with dimensions, (c) side view, (d) perspective view for a quarter region of the sub-array with dimensions.

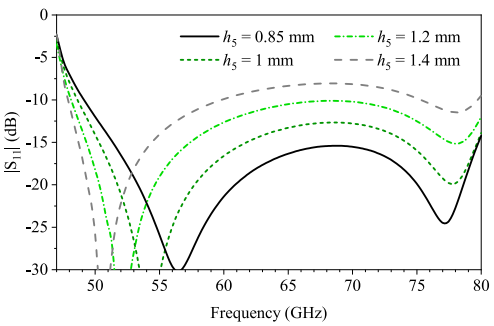

FIGURE 10. Simulated $|S_{11}|$ of the feed cavity of the sub-array for different h_5.

aperture size of $l_{horn} \times l_{horn}$, which are loaded with short sections of square waveguides with a height of h_1. The input ports of the horns are linked with vertical waveguides that act as the output ports of the feed cavity. As indicated in Fig. 9 (b), two triangular irises are cut in the cavity for impedance matching. Besides, the input waveguide port is in the center of the bottom surface of the cavity. In comparison with the sub-array designs reported previously in [44] and [46], two modifications are implemented in this work for achieving a better bandwidth performance. First, a portion of the feed cavity is bended upward to link with the vertical waveguides as shown in Fig. 9 (c), which makes it like a Y-shaped power divider in the *xoz*-plane with improved

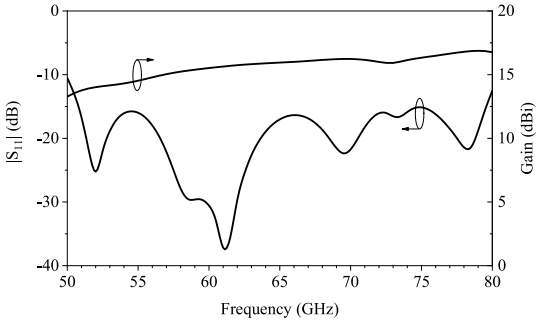

FIGURE 11. Comparison of the simulated $|S_{11}|$ and gain results of the proposed 2 × 2 sub-arrays.

TABLE 2. Dimensions of the 2 × 2 sub-array (unit: mm).

Parameters	a_1	b_1	h_1	h_2	h_3	h_4
Values	3.5	1.3	1	6.4	1	1.4
Parameters	h_5	h_{sp}	i_{h1}	i_{l1}	i_{w1}	i_{w2}
Values	0.85	2	0.9	1.4	0.8	1.65
Parameters	l_1	l_{horn}	l_{sp}	w_1	w_2	
Values	7.5	3.5	1.3	5.1	5	

impedance matching features. Second, an inverted pyramidal slit with a height of h_{sp} and a width of l_{sp} is cut at the center of the sub-array aperture. By this means, a portion of the common metallic walls for the four horn elements is removed. It is found that the existence of the slit is helpful to adjust the impedance matching characteristics of the sub-array, due to the reduction of the mutual coupling between the neighboring horn elements in the H-plane. The final dimensions of the proposed 2 × 2 sub-array are listed in Table 2.

Fig. 10 presents the simulated $|S_{11}|$ of the feed cavity whose output ports are connected with loads directly. It is seen that the height of the cavity h_5 is of importance to its matching characteristics. A simulated wide bandwidth of 43% for $|S_{11}|$ of less than −15 dB (from 51.5 to 79.9 GHz) is achieved by the cavity with $h_5 = 0.85$ mm. Furthermore, as illustrated in Fig. 11, the wideband features are not affected significantly when the matching loads are replaced with horn elements. The gain varies from 13.3 to 16.8 dBi throughout the operating band. Additionally, the simulated radiation patterns of the proposed sub-array drawn in Fig. 12 are symmetric and stable in both the E- and H- planes, while the cross polarization is less than −40 dB.

C. AIR-FILLED WAVEGUIDE X-JUNCTION

The air-filled waveguide X-junction constructing the X-type full-corporate feed network is shown in Fig. 13. The major portion of the X-junction is similar with the feed cavity used for 2 × 2 sub-arrays [36] and [44], in which the input power can be transmitted to four waveguides with an equal amplitude. The four waveguides are extended along ±45° directions and then connected with the vertical waveguides acting as the output ports. In order to get the required in-phase outputs, the upper two and the lower two vertical waveguides are located at the opposite sides of the planar

TABLE 3. Dimensions of the X-junctions (unit: mm).

Parameters	b_2	h_6	i_{l2}	i_{l3}	i_{l4}
1st X-junction	3.3	1	0.5	1.3	0.5
2nd X-junction	3.3	1	0.8	0.7	0.5
3rd X-junction	3.4	1	0.8	1	0.25
Parameters	i_{w3}	i_{w4}	l_2	l_3	l_4
1st X-junction	4	0.72	7.3	n.a.	1.3
2nd X-junction	1.5	0.65	7.4	3	4.9
3rd X-junction	1.5	0.8	7.4	10.4	12.2
Parameters	$offset_1$	$offset_2$	w_3	r_1	
1st X-junction	0.15	0.1	4.6	0.7	
2nd X-junction	0.2	0.4	4.8	0.5	
3rd X-junction	0.25	0.45	4.5	n.a.	

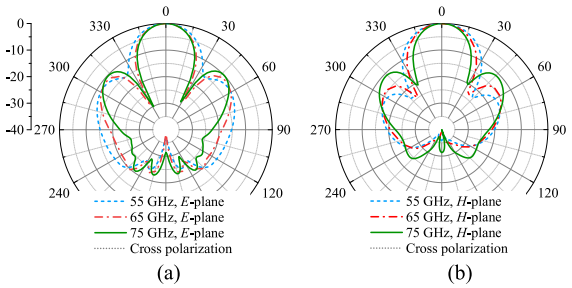

FIGURE 12. Simulated radiation patterns of the proposed 2 × 2 sub-array at 55, 65 and 75 GHz. (a) *E*-plane, (b) *H*-plane.

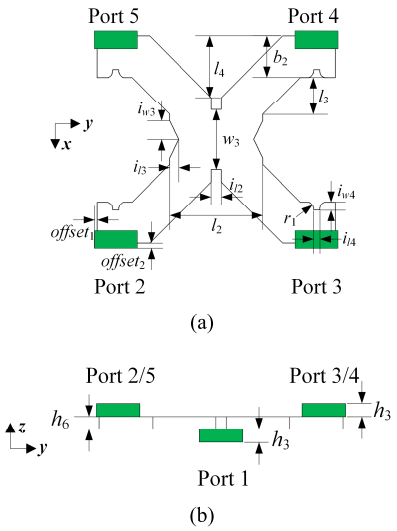

FIGURE 13. Geometry of the air-filled waveguide X-junction. (a) Top view with dimensions, (b) side view with dimensions.

waveguides. Besides, four irises are added at the shorted-ends of the planar waveguides for impedance matching. Detailed dimensions of the three types of X-junctions in the feed network are listed in Table 3.

The simulated S-parameters of the three X-junctions are illustrated in Fig. 14. An overlapped impedance bandwidth of 37% for the simulated $|S_{11}|$ of less than −10 dB (from 50 to 72.5 GHz) is obtained. By adopting the analysis process mentioned in Fig. 7, the combination of the designed

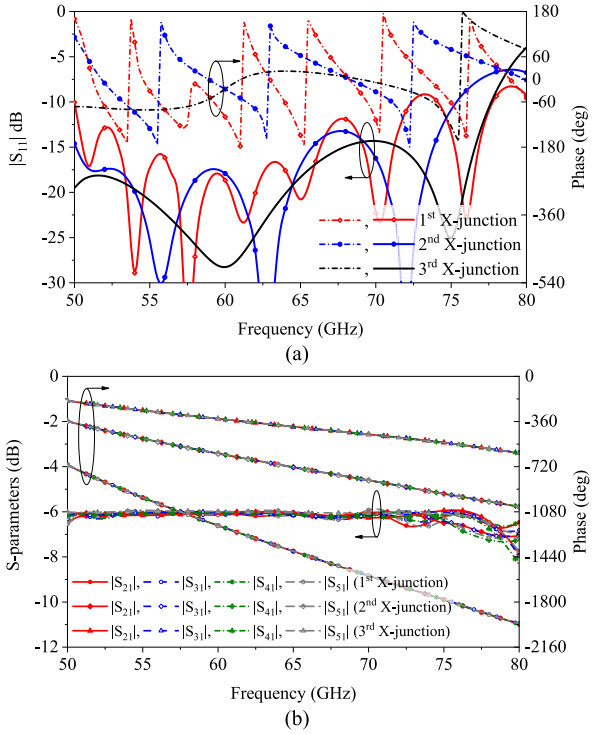

FIGURE 14. Simulated S-parameters of the 1st, 2nd and 3rd air-filled X-junctions. (a) Magnitudes and phases of S_{11}, (b) magnitudes and phases of S_{21} to S_{51}.

sub-arrays and the X-junctions is able to guarantee a reflection coefficient of less than −10 dB within the vicinities of 51 and 65.5 GHz for the proposed array. Moreover, the simulated magnitude and phase difference among the outputs are less than 0.2 dB and 4° in the frequency range between 50 and 73 GHz for the three X-junctions.

D. SIMULATED ARRAY PERFORMANCE

By combining the sub-arrays and the X-junctions presented above, the 8 × 8 and 16 × 16 horn antenna arrays fed by the X-type full-corporate feed networks are designed in the V-band, whose simulated $|S_{11}|$ and gain results are given in Fig. 15. Simulated impedance bandwidths of 40% (from 50.5 to 75.4 GHz) and 42% (from 50.8 to 77.7 GHz) for $|S_{11}|$ of lower than −10 dB are obtained by the 8 × 8 and 16 × 16 horn antenna arrays, respectively, which can almost cover the entire V-band. The simulated $|S_{11}|$ of the 16 × 16 array is still less than −10 dB at about 73.5 GHz even if $|S_{11}|$ of the 1st X-junction is slightly higher than −10 dB, which can be attributed to the partial reflection cancellation at the input port of the array caused by other two junctions. The wide bandwidths demonstrate the effectiveness of the proposed bandwidth enhancement scheme based on the X-type feed network. Furthermore, the simulated gain gradually increases with the frequency and is stable across the whole operating band for both of the arrays. The maximum gain results of the arrays are 28.0 and 33.6 dBi separately, while the variation is less than 4.5 dB throughout the operating band. The additional loss caused by the printed surface

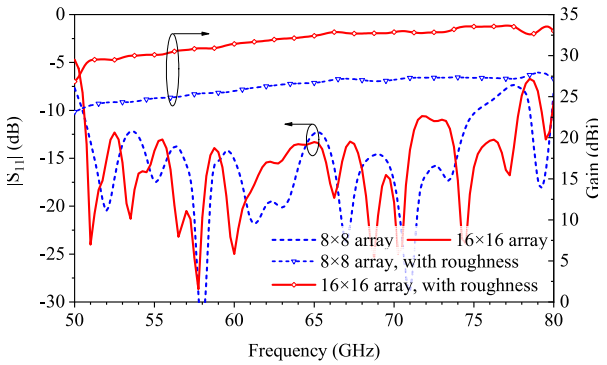

FIGURE 15. Simulated $|S_{11}|$ and gain results of the proposed wideband horn array antennas with sizes of 8 × 8 and 16 × 16.

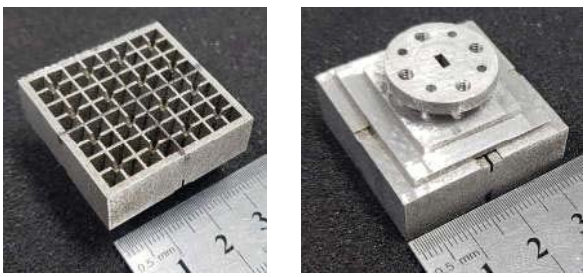

FIGURE 16. Photographs of the 3D printed 8 × 8 horn antenna array prototype. (a) Top view, (b) bottom view.

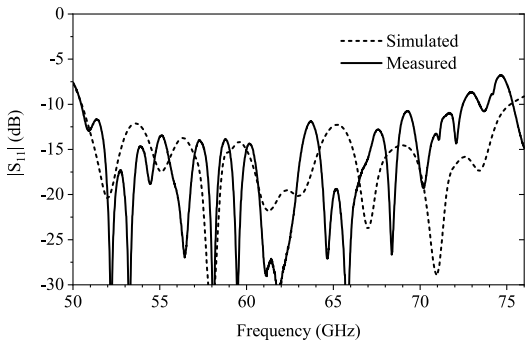

FIGURE 17. Measured and simulated $|S_{11}|$ of the 3D printed 8 × 8 horn antenna arrays.

roughness of about 10 μm [35] has been considered in the simulation.

IV. MEASUREMENT AND DISCUSSION

For experimentally verifying the operating characteristics, a prototype of the designed 8 × 8 horn antenna array shown in Fig. 16 was fabricated by employing a commercial 3D printing facility developed by EOS GmbH Company. The printing material is aluminum alloy AlSi10Mg powder. The resolution of the printing process is between 50 and 100 μm.

The overall size of the array is 34.5 × 34.5 × 21.8 mm^3. The input port of the array is a standard WR-15 waveguide located on the bottom surface. The reflection coefficient of the array was measured by using a Keysight PNA-X network analyzer N5247B with a V-band frequency extender N5293AX03. In addition, the radiation performance was measured in a far-field anechoic chamber. The gain of the array was calculated by comparing with a V-band standard gain horn.

A. S-PARAMETERS

The measured and simulated $|S_{11}|$ of the 8 × 8 horn antenna array are given in Fig. 17. The measured impedance bandwidth of less than −10 dB is 38% (from 50.5 to 73.9 GHz), which is in reasonable agreement with the simulated one of 40% (from 50.5 to 75.4 GHz). The satisfying bandwidth not only confirms the advantages of the proposed design method, but also demonstrates the feasibility of using commercial 3D printing technology for realizing V-band antenna arrays. The minor difference between measured and simulated results is mainly caused by the printing tolerance. Besides, it should be mentioned that the measured $|S_{11}|$ is slightly higher than −10 dB at 72.9 GHz.

B. RADIATION PATTERNS

A comparison between the measured and simulated radiation patterns of the 8 × 8 horn antenna array in the E- and H- planes at 55, 65 and 74 GHz are depicted in Fig. 18. The radiation patterns are symmetrical and stable in the two planes orthogonal to each other over the operating band. The first sidelobe level is around −13 dB, which is close to the theoretical value for the array with a uniform aperture distribution.

Moreover, it can be seen that there are some discrepancies between the measured and simulated sidelobe levels for the angle of larger than 45°. The possible reasons are explained below. By comparing the fabricated prototype with the designed model, it is found that the printed horn aperture size is slightly smaller than the simulated one, which would affect the aperture field distribution and thus varying the sidelobe. Besides, the measurement setup close to the antenna under test may also influence the radiation pattern in the large angle directions. In addition, the measured cross polarization of the proposed horn array is less than −32 dB.

C. GAIN AND EFFICIENCY

Fig. 19 shows the measured and simulated gain curves and the simulated directivity of the array. The measured and simulated gains of the printed 8 × 8 horn antenna array are up to 27.8 and 27.9 dBi with variations of 3.6 and 3.7 dB over the operating band, respectively. An extra metallic loss of around 0.56 dB caused by the surface roughness can be observed by employing Hall-Huary model in the simulation [47]. In addition, by comparing the measured gain with simulated directivity, the estimated radiation efficiency of the array is about 89%, which is comparable with the previous results of the 3D printed array in the Ka-band [44]. Besides, by comparing the simulated directivity of the array with the

TABLE 4. Comparisons between the proposed and reported millimeter-wave wideband antenna arrays with air-filled feed network.

Ref.	Fabrication technology	Antenna element	Full-corporate feed network	Antenna element BW	Power divider BW	Array size	f_0 (GHz)	BW	Max. gain (dBi)	Max. radiation efficiency
[20]	MEMS micromachining	Horn	H-type (Waveguide)	29%	29%	16 × 16	140	29%	33.2	70.9%
[32]	Milling	Slot	H-type (Ridge gap waveguide)	30%	30%	8 × 8	59	30%	27.5	n.a.
[36]	3D printing	ME-dipole	H-type (Stepped waveguide)	54%	65%	8 × 8	34	31%	28.5	89%
This work	3D printing	Horn	X-type (Waveguide)	43%	37%	8 × 8	63	38%	27.8	89%
						16 × 16	64	42% (sim.)	33.6 (sim.)	83% (sim.)

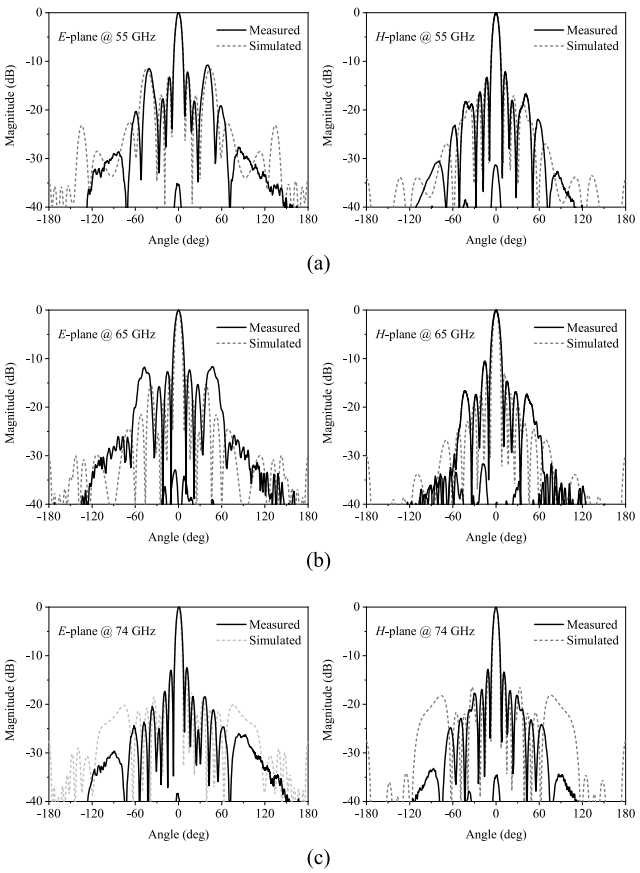

FIGURE 18. Measured and simulated radiation patterns of the 3D printed 8 × 8 horn antenna array. (a) $f = 55$ GHz, (b) $f = 65$ GHz, (c) $f = 74$ GHz.

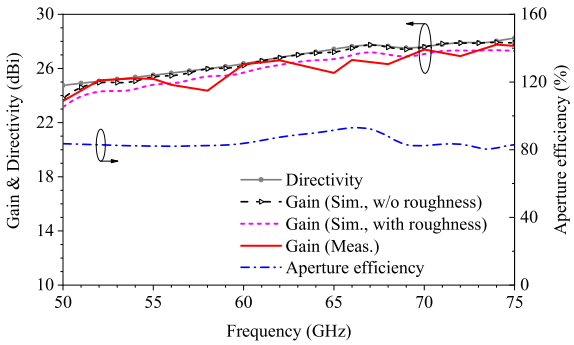

FIGURE 19. Gain, directivity and aperture efficiency of the 3D printed 8 × 8 horn antenna array.

maximum achievable directivity, the aperture efficiency of the array is larger than 80% over the operating band.

D. COMPARISON AND DISCUSSION

Geometrical and operating characteristics of the proposed and reported millimeter-wave wideband high-gain antenna arrays with air-filled full-corporate feed networks are summarized in Table 4. It is seen that the H-type full-corporate feed networks were adopted by the reported arrays. The bandwidths of the arrays in [20] and [32] are similar with those of antenna elements and power dividers composing the arrays. However, even though the bandwidths of the antenna elements and power dividers are improved to more than 50% in [36], the bandwidth of the array is still about 30%. Furthermore, by employing the proposed bandwidth enhancement scheme based on the X-type feed network, the bandwidth of the millimeter-wave high-gain array can be promoted significantly to around 40%. Meanwhile, benefitted from the X-junctions having a simple geometry, the tiny irises for the impedance matching of the wideband T-junctions in [36] are saved such that the requirement for the minimum printable dimension in the 3D printing process can be met in the V-band. The satisfying measured results of the printed prototype confirm the feasibility of realizing wideband high-gain antenna arrays operating at 60-GHz by using the commercial 3D printing technology.

In terms of the gain and radiation efficiency, because of a shorter transmission path in the presented X-type feed network compared with the counterpart in the H-type one with the same size, the metallic loss of the feed network can be reduced as well. Hence, the radiation efficiencies of the proposed arrays operating at higher frequencies are still comparable with the results of the reported Ka-band array in [36].

V. CONCLUSION

A bandwidth enhancement scheme for the millimeter-wave high-gain antenna arrays with large sizes has been investigated by using a one-time-reflection model of the antenna array with full-corporate feed networks. It has been explored that benefitted from the weaker in-phase reflection superposition and the shorter transmission path length, a wider bandwidth can be achieved by the proposed X-type full-corporate feed network. Based on the analysis, novel 60-GHz 3D printed horn arrays composed of wideband subarrays and air-filled X-junctions have been designed. Wide bandwidths of about 40%, stable radiation patterns over the operating bands and high-gain performance have been achieved by the arrays with sizes of 8×8 and 16×16. Taking advantage of the simple geometry that can be printed in a whole piece, the improved bandwidth, and the promising radiation characteristics, the presented design method and antenna array are attractive for the advanced millimeter-wave wideband communications.

REFERENCES

[1] W. Sun, Y. Li, L. Chang, H. Li, X. Qin, and H. Wang, "Dual-band dual-polarized microstrip antenna array using double-layer gridded patches for 5G millimeter-wave applications," *IEEE Trans. Antennas Propag.*, vol. 69, no. 10, pp. 6489–6499, Oct. 2021.

[2] J. Wang *et al.*, "A low-profile vertically polarized magneto-electric monopole antenna with a 60% bandwidth for millimeter-wave applications," *IEEE Trans. Antennas Propag.*, vol. 69, no. 1, pp. 3–13, Jan. 2021.

[3] J. Wang, Y. Li, F. Wu, D. Jiang, and J. Wang, "Millimeter-wave wideband endfire magnetoelectric dipole antenna fed by substrate integrated coaxial line," *IEEE Trans. Antennas Propag.*, vol. 70, no. 3, pp. 2301–2306, Mar. 2022.

[4] H. Li, Y. Li, L. Chang, W. Sun, X. Qin, and H. Wang, "A wideband dual-polarized endfire antenna array with overlapped apertures and small clearance for 5G millimeter-wave applications," *IEEE Trans. Antennas Propag.*, vol. 69, no. 2, pp. 815–824, Feb. 2021.

[5] D. X. Liu, B. Gaucher, U. Pfeiffer, and J. Grzyb, *Advanced Millimeter-Wave Technologies, Antennas, Packaging and Circuits*. Hoboken, NJ, USA: Wiley, 2009.

[6] A. E. I. Lamminen, J. Saily, and A. R. Vimpari, "60-GHz patch antennas and arrays on LTCC with embedded-cavity substrates," *IEEE Trans. Antennas Propag.*, vol. 56, no. 9, pp. 2865–2874, Sep. 2008.

[7] L. Wang, Y.-X. Guo, and W.-X. Sheng, "Wideband high-gain 60-GHz LTCC L-probe patch antenna array with a soft surface," *IEEE Trans. Antennas Propag.*, vol. 61, no. 4, pp. 1802–1809, Apr. 2013.

[8] M. H. Awida, S. H. Suleiman, and A. E. Fathy, "Substrate-integrated cavity-backed patch arrays: A low-cost approach for bandwidth enhancement," *IEEE Trans. Antennas Propag.*, vol. 59, no. 4, pp. 1155–1163, Apr. 2011.

[9] Y. Li and K. Luk, "60-GHz substrate integrated waveguide fed cavity-backed aperture-coupled microstrip patch antenna arrays," *IEEE Trans. Antennas Propag.*, vol. 63, no. 3, pp. 1075–1085, Mar. 2015.

[10] E. Levine, G. Malamud, S. Shtrikman, and D. Treves, "A study of microstrip array antennas with the feed network," *IEEE Trans. Antennas Propag.*, vol. 37, no. 4, pp. 426–434, Apr. 1989.

[11] Y. Li, Z. N. Chen, X. Qing, Z. Zhang, J. Xu, and Z. Feng, "Axial ratio bandwidth enhancement of 60-GHz substrate integrated waveguide-fed circularly polarized LTCC antenna array," *IEEE Trans. Antennas Propag.*, vol. 60, no. 10, pp. 4619–4626, Oct. 2012.

[12] D.-F. Guan, C. Ding, Z.-P. Qian, Y.-S. Zhang, Y. J. Guo, and K. Gong, "Broadband high-gain SIW cavity-backed circular-polarized array antenna," *IEEE Trans. Antennas Propag.*, vol. 64, no. 4, pp. 1493–1497, Apr. 2016.

[13] Y. Li and K. Luk, "A 60-GHz wideband circularly polarized aperture-coupled magneto-electric dipole antenna array," *IEEE Trans. Antennas Propag.*, vol. 64, no. 4, pp. 1325–1333, Apr. 2016.

[14] W. Lin, R. W. Ziolkowski, and T. C. Baum, "28 GHz compact omnidirectional circularly polarized antenna for device-to-device communications in the future 5G systems," *IEEE Trans. Antennas Propag.*, vol. 65, no. 12, pp. 6904–6914, Dec. 2017.

[15] Y. Miura, J. Hirokawa, M. Ando, Y. Shibuya, and G. Yoshida, "Double-layer full-corporate-feed hollow-waveguide slot array antenna in the 60-GHz band," *IEEE Trans. Antennas Propag.*, vol. 59, no. 8, pp. 2844–2851, Aug. 2011.

[16] Z. Shi-Gang, H. Guan-Long, P. Zhao-Hang, and L. Ying, "A wideband full-corporate-feed waveguide slot planar array," *IEEE Trans. Antennas Propag.*, vol. 64, no. 5, pp. 1974–1978, May 2016.

[17] A. Farahbakhsh, D. Zarifi, and A. U. Zaman, "60-GHz groove gap waveguide based wideband H-plane power dividers and transitions: For use in high-gain slot array antenna," *IEEE Trans. Microw. Theory Tech.*, vol. 65, no. 11, pp. 4111–4121, Nov. 2017.

[18] L. Chang, Y. Li, Z. Zhang, S. Wang, and Z. Feng, "Planar air-filled terahertz antenna array based on channelized coplanar waveguide using hierarchical silicon bulk micromachining," *IEEE Trans. Antennas Propag.*, vol. 66, no. 10, pp. 5318–5325, Oct. 2018.

[19] Z. Qi, X. Li, J. Xiao, and H. Zhu, "Low-cost empty substrate integrated waveguide slot arrays for millimeter-wave applications," *IEEE Antennas Wireless Propag. Lett.*, vol. 18, no. 5, pp. 1021–1025, May 2019.

[20] S. S. Yao, Y. J. Cheng, M. M. Zhou, Y. F. Wu, and Y. Fan, "D-band wideband air-filled plate array antenna with multistage impedance matching based on MEMS micromachining technology," *IEEE Trans. Antennas Propag.*, vol. 68, no. 6, pp. 4502–4511, Jun. 2020.

[21] X. Chen, K. Wu, L. Han, and F. He, "Low-cost high gain planar antenna array for 60-GHz band applications," *IEEE Trans. Antennas Propag.*, vol. 58, no. 6, pp. 2126–2129, Jun. 2010.

[22] J. Xu, Z. N. Chen, X. Qing, and W. Hong, "Bandwidth enhancement for a 60 GHz substrate integrated waveguide fed cavity array antenna on LTCC," *IEEE Trans. Antennas Propag.*, vol. 59, no. 3, pp. 826–832, Mar. 2011.

[23] B. Zhang and Y. P. Zhang, "Grid array antennas with subarrays and multiple feeds for 60-GHz radios," *IEEE Trans. Antennas Propag.*, vol. 60, no. 5, pp. 2270–2275, May 2012.

[24] X. Bai, S.-W. Qu, and K. B. Ng, "Millimeter-wave cavity-backed patch-slot dipole for circularly polarized radiation," *IEEE Antennas Wireless Propag. Lett.*, vol. 12, pp. 1355–1358, 2013.

[25] P.-F. Li, S. Liao, Q. Xue, and S.-W. Qu, "60 GHz dual-polarized high-gain planar aperture antenna array based on LTCC," *IEEE Trans. Antennas Propag.*, vol. 68, no. 4, pp. 2883–2894, Apr. 2020.

[26] Y. Li and K. Luk, "Low-cost high-gain and broadband substrate-integrated-waveguide-fed patch antenna array for 60-GHz band," *IEEE Trans. Antennas Propag.*, vol. 62, no. 11, pp. 5531–5538, Nov. 2014.

[27] Q. Zhu, K. B. Ng, C. H. Chan, and K. Luk, "Substrate-integrated-waveguide-fed array antenna covering 57–71 GHz band for 5G applications," *IEEE Trans. Antennas Propag.*, vol. 65, no. 12, pp. 6298–6306, Dec. 2017.

[28] Z. Chen, H. Liu, J. Yu, and X. Chen, "High gain, broadband and dual-polarized substrate integrated waveguide cavity-backed slot antenna array for 60 GHz band," *IEEE Access*, vol. 6, pp. 31012–31022, 2018.

[29] Y. Zhao and K. Luk, "Dual circular-polarized SIW-fed high-gain scalable antenna array for 60 GHz applications," *IEEE Trans. Antennas Propag.*, vol. 66, no. 3, pp. 1288–1298, Mar. 2018.

[30] K. Fan, Z. Hao, Q. Yuan, G. Q. Luo, and W. Hong, "A wideband high-gain planar integrated antenna array for E-band backhaul applications," *IEEE Trans. Antennas Propag.*, vol. 68, no. 3, pp. 2138–2147, Mar. 2020.

[31] Q. Wu, J. Hirokawa, J. Yin, C. Yu, H. Wang, and W. Hong, "Millimeter-wave planar broadband circularly polarized antenna array using stacked curl elements," *IEEE Trans. Antennas Propag.*, vol. 65, no. 12, pp. 7052–7062, Dec. 2017.

[32] A. Farahbakhsh, D. Zarifi, and A. U. Zaman, "A mm-Wave wideband slot array antenna based on ridge gap waveguide with 30% bandwidth," *IEEE Trans. Antennas Propag.*, vol. 66, no. 2, pp. 1008–1013, Feb. 2018.

[33] P. Liu, G. F. Pedersen, and S. Zhang, "Wideband slot array antenna fed by open-ended rectangular waveguide at W-band," *IEEE Antennas Wireless Propag. Lett.*, vol. 21, no. 4, pp. 666–670, Apr. 2022.
[34] A. Gomez-Torrent *et al.*, "A 38 dB gain, low-loss, flat array antenna for 320–400 GHz enabled by silicon-on-insulator micromachining," *IEEE Trans. Antennas Propag.*, vol. 68, no. 6, pp. 4450–4458, Jun. 2020.
[35] F. Sun, Y. Li, L. Ge, and J. Wang, "Millimeter-wave magneto-electric dipole antenna array with a self-supporting geometry for time-saving metallic 3-D printing," *IEEE Trans. Antennas Propag.*, vol. 68, no. 12, pp. 7822–7832, Dec. 2020.
[36] Y. Li *et al.*, "A Ka-band 3-D-printed wideband stepped waveguide-fed magnetoelectric dipole antenna array," *IEEE Trans. Antennas Propag.*, vol. 68, no. 4, pp. 2724–2735, Apr. 2020.
[37] F. Sun *et al.*, "A millimeter-wave wideband dual-polarized antenna array with 3-D-printed air-filled differential feeding cavities," *IEEE Trans. Antennas Propag.*, vol. 70, no. 2, pp. 1020–1032, Feb. 2022.
[38] Q. You, Y. Lu, Y. You, Y. Wang, Z. Hao, and J. Huang, "Wideband full-corporate-feed waveguide continuous transverse stub antenna array," *IEEE Access*, vol. 6, pp. 76673–76681, 2018.
[39] K. Ding and A. A. Kishk, "Multioctave bandwidth of parallel-feeding network based on impedance transformer concept," *IEEE Trans. Antennas Propag.*, vol. 67, no. 4, pp. 2803–2808, Apr. 2019.
[40] Y. Li, C. Wang, and Y. X. Guo, "A Ka-band wideband dual-polarized magnetoelectric dipole antenna array on LTCC," *IEEE Trans. Antennas Propag.*, vol. 68, no. 6, pp. 4985–4990, Jun. 2020.
[41] D. M. Pozar, *Microwave Engineering*, 4th ed. Hoboken NJ, USA: Wiley, 2001, pp. 250–252.
[42] B. Zhang *et al.*, "Metallic 3-D printed antennas for millimeter-and sub-millimeter wave applications," *IEEE Trans. THz Sci. Technol.*, vol. 6, no. 4, pp. 592–600, Jul. 2016.
[43] G.-L. Huang, S.-G. Zhou, T.-H. Chio, and T.-S. Yeo, "Fabrication of a high-efficiency waveguide antenna array via direct metal laser sintering," *IEEE Antennas Wireless Propag. Lett.*, vol. 15, pp. 622–625, 2016.
[44] Y. Li *et al.*, "3-D printed high-gain wideband waveguide fed horn antenna arrays for millimeter-wave applications," *IEEE Trans. Antennas Propag.*, vol. 67, no. 5, pp. 2868–2877, May 2019.
[45] (Ansoft Corp., Canonsburg, PA, USA). *HFSS: High Frequency Structure Simulator Based on the Finite Element Method*. [Online]. Available: http://www.ansoft.com/
[46] F. Sun, Y. Li, and J. Wang, "3D printed 60-GHz high-gain horn antenna arrays with 40% bandwidth," in *Proc. IEEE Asia-Pacific Microw. Conf.*, 2020, pp. 480–482.
[47] B. Simonovich, "Practical method for modeling conductor surface roughness using close packaging of equal spheres," in *Proc. Design Conf.*, Santa Clara, CA, USA, 2015, pp. 1–62.

FANQI SUN (Student Member, IEEE) was born in Jilin, China, in 1994. She received the B.E. degree from the School of Electronic and Information Engineering, Beijing Jiaotong University, Beijing, China, in 2017, where she is currently pursuing the Ph.D. degree in electronic engineering.

Her current research interests include millimeter-wave antennas and arrays.

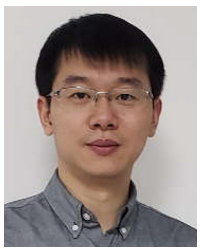

YUJIAN LI (Member, IEEE) was born in Hunan, China, in 1987. He received the B.S. and M.S. degrees in communications engineering from Beijing Jiaotong University, Beijing, China, in 2009 and 2012, respectively, and the Ph.D. degree in electronic engineering from the City University of Hong Kong in 2015.

In 2015, he joined the Institute of Lightwave Technology, Beijing Jiaotong University, where he is currently a Full Professor with the School of Electronic and Information Engineering. His current research interests include millimeter-wave antennas, base station antennas, and leaky wave structures.

Dr. Li was awarded the Outstanding Research Thesis Award from the City University of Hong Kong in 2015. He received the Best Paper Award at the 2015 IEEE Asia–Pacific Conference on Antennas and Propagation, the Best Student Paper at 2013 National Conference on Antennas, and the Best Student Paper Award (2nd Prize) at the 2013 IEEE International Workshop on Electromagnetics. He was selected as a Finalist in the Student Paper Contest of 2015 IEEE AP-S Symposium on Antennas and Propagation. He has served as a Reviewer for the IEEE TRANSACTIONS ON ANTENNAS AND PROPAGATION, the IEEE ANTENNAS AND WIRELESS PROPAGATION LETTERS, and the *IET Microwaves, Antennas & Propagation*.

JUNHONG WANG (Senior Member, IEEE) was born in Jiangsu, China, in 1965. He received the B.S. and M.S. degrees in electrical engineering from the University of Electronic Science and Technology of China, Chengdu, China, in 1988 and 1991, respectively, and the Ph.D. degree in electrical engineering from Southwest Jiaotong University, Chengdu, in 1994. In 1995, he joined as a Faculty Member with the Department of Electrical Engineering, Beijing Jiaotong University, Beijing, China, where he became a Professor in 1999. From January 1999 to June 2000, he was a Research Associate with the Department of Electrical Engineering, City University of Hong Kong, Hong Kong. From July 2002 to July 2003, he was a Research Scientist with the Temasek Laboratories, National University of Singapore, Singapore. He is currently with the Key Laboratory of All Optical Network and Advanced Telecommunication Network, Ministry of Education, Beijing Jiaotong University, where he is also with the Institute of Lightwave Technology. His research interests include numerical methods, antennas, scattering, and leaky wave structures.

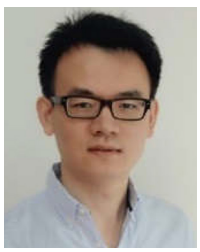

LEI GE (Senior Member, IEEE) was born in Jiangsu, China. He received the B.S. degree in electronic engineering from the Nanjing University of Science and Technology, Nanjing, China, in 2009, and the Ph.D. degree in electronic engineering from the City University of Hong Kong, Hong Kong, in 2015.

From September 2010 to July 2011, he was a Research Assistant with the City University of Hong Kong. From April 2015 to October 2015, he was a Postdoctoral Research Fellow with the State Key Laboratory of Millimeter Waves, City University of Hong Kong. He is currently an Assistant Professor and an Associate Head of the Department of Electronic Engineering, Shenzhen University, China. His recent research interests focus on wideband antennas, patch antennas, base station antennas, reconfigurable antennas, the antennas for cognitive radio, and filtering antennas. He received the Honorable Mention at the Student Contest of 2012 IEEE APS-URSI Conference and Exhibition held in Chicago, USA. He won the First Prize in the Student Innovation Competition of 2014 IEEE International Workshop on Electromagnetics (IEEE iWEM) held in Sapporo, Japan, in 2014. He was the Session Chair of the iWEM 2017 and ACES-China 2017. He was the TPC Member of the APCAP 2016.

JIANXIN CHEN (Senior Member, IEEE) was born in Nantong, Jiangsu, China, in 1979. He received the B.S. degree from Huaiyin Teachers College, Jiangsu, in 2001, the M.S. degree from the University of Electronic Science and Technology of China, Chengdu, China, in 2004, and the Ph.D. degree from the City University of Hong Kong, Hong Kong, in 2008.

Since 2009, he has been with Nantong University, Jiangsu, where he is currently a Professor. He has authored or coauthored more than 80 internationally referred journal and conference papers. He holds three Chinese patents and two U.S. patents. His research interests include microwave active/passive circuits and antennas, and LTCC-based millimeter-wave circuits and antennas. He was the recipient of the Best Paper Award presented at the Chinese National Microwave and Millimeter-Wave Symposium, Ningbo, China, in 2007. He was a Supervisor of 2014 iWEM Student Innovation Competition Winner in Sapporo, Japan.

WEI QIN (Member, IEEE) was born in Jiangsu, China. He received the B.Sc. degree in electronic engineering and the M.Sc. degree in electromagnetics and microwave technology from Southeast University, Nanjing, China, in 2007 and 2010, respectively, and the Ph.D. degree in electronic engineering from the City University of Hong Kong, Hong Kong, China, in 2013.

From July 2013 to November 2013, he was a Senior Research Associate with the State Key Laboratory of Millimeter Waves, City University of Hong Kong. Since 2014, he has been with the School of Information Science and Technology, Nantong University, Nantong, Jiangsu, China, where he is currently a Professor. His research interest focuses on deign and application of microwave devices and antennas.